AFR-Based Fuel Ethanol Content Estimation in Flex-Fuel Engines Tolerant to MAF Sensor Drifts

Kyung-ho Ahn, Anna G. Stefanopoulou, *Fellow, IEEE*, and Mrdjan Jankovic, *Fellow, IEEE*

***Abstract*—Flexible fuel vehicles (FFVs) can operate on a blend of ethanol and gasoline in any volumetric concentration of up to 85% ethanol (93% in Brazil). Existing FFVs rely on ethanol sensor installed in the vehicle fueling system, or on an ethanol estimation based on air-to-fuel ratio (AFR) regulation via an exhaust gas oxygen (EGO) or λ sensor. The EGO-based ethanol detection is desirable from cost and maintenance perspectives but it is known to be prone to large errors during mass air flow sensor drifts. Ethanol content estimation can be realized by a feedback-based fuel correction of the feedforward-based fuel calculation using an exhaust gas oxygen sensor. When the fuel correction is attributed to the difference in stoichiometric air-to-fuel ratio (SAFR) between ethanol and gasoline, it can be used for ethanol estimation. When the fuel correction is attributed to a mass air flow (MAF) sensor error, it can be used for sensor drift estimation and correction. Deciding under which condition to blame (and detect) ethanol and when to switch to sensor correction burdens the calibration of FFV engine controllers. Moreover, erroneous decisions can lead to biases in ethanol estimation and in MAF sensor correction. In this paper, we present AFR-based ethanol content estimation, associated sensitivity and dynamical analysis, and a cylinder air flow estimation scheme that accounts for MAF sensor drift or bias using an intake manifold absolute pressure (MAP) sensor. The proposed fusion of the MAF, MAP, and λ sensor measurements prevents severe misestimation of ethanol content in flex fuel vehicles.**

***Index Terms*—Automotive fault detection, engine control, estimation, sensor drift.**

NOMENCLATURE

AFR_s	Stoichiometric air-to-fuel ratio.
C	MAF sensor drift parameter.
e	Volume fraction of ethanol in a fuel blend.
e_m	Mass fraction of ethanol in a fuel blend.
p_m	Intake manifold absolute pressure.
R	Gas constant.
T_m	Intake manifold temperature.
V_d	Total displaced cylinder volume.
V_m	Intake manifold volume.
W_{cyl}	Air flow rate into the cylinder.
W_{fb}	Feedback fuel flow command.
W_{ff}	Feedforward fuel flow command.
W_{ff1}	Feedforward fuel flow command not compensated by the fuel puddle dynamics.
W_θ	Air flow rate through the throttle.

Greek:

α_{tr}	Switching signal between ethanol adaptation and others.
β_{tr}	Switching signal in MAF sensor drift adaptation.
η_v	Volumetric efficiency.
θ	Throttle angle.
λ	Ratio of actual AFR to stoichiometric AFR.
τ_{MAF}	MAF sensor time constant.

I. INTRODUCTION

PETROLEUM-BASED fossil fuels are the dominant energy source for transportation. Recently, however, ethanol is being increasingly used as a fuel additive to support carbon-neutral transportation. The advantage of ethanol, among others, is that it is a renewable fuel produced from biomass such as barley, corn, wheat, sugar cane, trees and grasses. As mandated by the US government Energy Policy Act of 2005 (EPACT2005), 7.5 billion gallons of bio-fuel will be produced in 2012 to reduce dependence on fossil fuels. Currently available flexible fuel vehicles can operate on a blend of ethanol and gasoline in any concentration of up to 85% ethanol. This blend is denoted by the EXX nomenclature, where XX represents the volumetric percentage of ethanol in the blend. In the United States, E85 is commonly used as an alternative to normal gasoline fuel.[1] Flexible fuel vehicles are currently being offered by many manufacturers.

The characteristics of ethanol differ from those of gasoline, as shown in Table I. The influence of ethanol fuel on a spark ignition engine, which are induced by the different properties from those of gasoline, are well reported in [2]. Often ethanol fuel is associated with driveability and startability problems in cold and hot weather [3], [4] and at high altitude [5]. Existing FFVs achieve lower range (miles driven per tank) when operating on high ethanol content fuel due to its lower combustion heating value as compared to gasoline. However, as shown in

Manuscript received January 23, 2011; revised August 01, 2011; accepted January 22, 2012. Manuscript received in final form February 08, 2012. Date of publication April 03, 2012; date of current version nulldate. This work was supported by funds provided from a UMICH/Ford Alliance grant. Recommended by Associate Editor J. Y. Lew.

K.-H. Ahn is with the Hyundai-Kia Motors R&D Center, Hwaseong, Gyeonggi-do 445-706, South Korea (e-mail: kahn95@gmail.com).

A. G. Stefanopoulou is with the Department of Mechanical Engineering, University of Michigan, Ann Arbor, MI 48109-2121 USA (annastef@umich.edu).

M. Jankovic is with the Ford Research and Advanced Engineering, Dearborn, MI 48121 USA (e-mail: mjankov1@ford.com).

Color versions of one or more of the figures in this paper are available online at http://ieeexplore.ieee.org.

Digital Object Identifier 10.1109/TCST.2012.2187786

[1] In Brazil, however, a fuel blend called E100 is a blend of 93% ethanol and 7% of water [1]. Water-ethanol fuel blends are not considered in this paper.

TABLE I
PROPERTIES OF ETHANOL COMPARED WITH GASOLINE

Property	Gasoline	Ethanol
Research Octane Number (RON)	92	111
Density ($\mathrm{kg/m^3}$)	747	789
Heat of combustion (MJ/kg)	42.4	26.8
Stoichiometric air-to-fuel ratio	14.6	9.0
Boiling point (°C)	20–300	78.5
Latent heat of vaporization (kJ/kg)	420	845

Table I, ethanol has a higher octane ratio and therefore, a higher compression ratio and higher combustion efficiency can be obtained without knocking problems. Another advantage is that, the high vaporization heat can be used for charge cooling [6], which can further improve the knock resistance and potentially fuel economy. Given the effect of fuel variation, flexible fuel vehicles (FFVs) should embed engine calibration maps in their controllers and management systems to account for this variation. Calibration in an optimized flex-fuel strategy involves reliably estimating the ethanol percentage. Although this estimation is possible with the addition of a di-electric or electrochemical ethanol concentration sensor in the fueling system, the reliability and the cost of these sensors might prevent their use. Apart from the cost and reliability issues associated with such sensors, on-board diagnostic (OBD) requirements would require a redundant method independent of the fuel sensor for assessing the ethanol percent in order to diagnose the ethanol sensor faults or degradation.

Typically ethanol content estimation is initiated after the detection of refueling. This estimation is achieved using an exhaust gas oxygen (EGO) sensor which calculates the air-to-fuel ratio (AFR) under the assumption of stoichiometric conditions given the closed loop control of fuel injection with the feedback of λ measurements. For example, an increased fuel ethanol content (say, E40 instead of E0), hence decreased stoichiometric air-to-fuel ratio ($\mathrm{AFR}_s = 12.5$ instead of 14.6) according to Table I would cause lean ($\lambda = 1.4$ instead of 1.0) EGO sensor measurement. Due to the feedback control, the fuel injection amount increases to reach again the stoichiometric condition ($\lambda = 1$). This increase is recognized as decreased AFR_s and hence the stoichiometric air-to-fuel ratio (SAFR)-based ethanol estimation, called SAFR ethanol from now on, is interpreted as increased fuel ethanol content. The refueling event trigger is used to avoid misclassifying ethanol content variations as actuator faults (drifts) or component aging.

Since the ethanol content estimation relies on the AFR calculated using the cylinder air charge estimation and issued fuel amount, the ethanol estimation will erroneously compensate for the air charge estimation error and/or fuel injector error.

The ethanol estimation is very sensitive to fuel injection errors [7] and will be treated in a separate publication since it requires integration with the estimation of fuel injection error as in [8] and [9] for flex-fuel direct injection (DI) engines equipped with in-cylinder pressure sensors. In this paper, the fuel injection system is considered faultless and well-calibrated, and the focus is on the ethanol estimation during errors arising in the air-flow path due to MAF sensor drifts.

If the ethanol content or the stoichiometric AFR is known, the EGO sensor reading may be used in another adaptation against MAF sensor drift/bias in the same manner as used in ethanol content estimation. In other words, the calculated AFR can be used to update a parameter in the air charge estimation with respect to the fixed stoichiometric AFR. The use of EGO-based fuel feedback compensation to adapt the feedforward fuel compensation in response to errors in the inlet air sensing is now a common practice [10] referred as air charge adaptation. It is necessary to switch between two adaptations namely, the ethanol adaptation and the air charge adaptation, to avoid misclassifying ethanol content variations as sensor drifts or component aging. An appropriate switching logic using the tank refill trigger and relevant process characteristics should be devised for that purpose. However, this scheme may cause unobservable biases in estimations because every estimation is dependent on the true value of other estimations to guarantee convergence to its actual value. Convergence of estimations to actual values is important even though there are no true or reference values to which all estimations can be reset, once a vehicle leaves the factory or undergoes a major maintenance event unless the vehicle operates with known fuel. This estimation bias during regular field operation will be briefly discussed in Section III-A.

In this paper, first, a simple stoichiometric AFR estimation law using the exhaust oxygen sensor is proposed, analyzed and discussed in light of closed loop regulation of stoichiometric condition. This law yields the estimated ethanol percentage in the fuel. This article then focuses on the cylinder air flow estimation under MAF sensor drift or bias using an intake manifold absolute pressure (MAP) sensor in order to prevent severe misestimation of ethanol content in flex fuel vehicles [11]. The estimation scheme is independent of the exhaust gas oxygen sensor measurement which is used for ethanol content update via the closed loop regulation of stoichiometric condition. Therefore, the switching between this compensation of MAF sensor drift and the ethanol content estimation is not necessary and the associated estimation bias problem can be avoided. Simulations are performed to characterize the ethanol content estimation algorithm quantifying various sensitivities and to demonstrate the air flow estimation with compensation of MAF sensor drift using a MAP sensor realizing robust ethanol content estimation in flex fuel vehicles.

II. ETHANOL CONTENT ESTIMATION

This section provides the basic AFR-based ethanol content estimation algorithm. The principle is first described assuming a perfect AFR regulation at its stoichiometric value with the use of a λ sensor. Air-to-fuel ratio control around the stoichiometric ratio of a fuel blend is important for the operation of the catalytic converter. The majority of gasoline engine powertrains rely on this regulation which is typically achieved by a combination of feedforward and feedback fuel injection control. The feedback controller is based on the measured ratio (λ) of the actual air-to-fuel ratio (AFR) to the stoichiometric ratio (AFR_s) through an exhaust gas oxygen sensor. The λ ratio is compared to $\lambda^{\mathrm{des}} = 1$ and the error is used by a proportional-integral (PI) controller to adjust the feedback fuel command. Despite all the modeling and control design efforts, the λ regulation is not perfect during

transients. The ethanol estimation could, hence, rely on heavily filtered signals compromising speed of response for accuracy.

At first glance the importance of accuracy and the frequency of refueling event may lead to an assumption that speed of response can be easily sacrificed. But the ethanol detection period also needs to be as short as possible to reduce the probability of stopping the car and letting it cool down without a correct ethanol estimation having been established. This possibility is undesirable since the cold start depends heavily on correct ethanol estimation.[2] It is hence necessary to thoroughly understand and develop models to address how the interconnected dynamics of the AFR regulation and the ethanol estimation propagate through the detection process and can be tuned.

A. Principle of SAFR Ethanol Estimation

Given an accurate and fast regulation of λ to its desired value $\lambda^{\mathrm{des}} = 1$, the stoichiometric value (AFR_s) can be calculated from the ratio of the measured mass air flow $\overline{W}_\theta$ and the known injected fuel mass flow W_{inj}

$$\widehat{\mathrm{AFR}}_s = \frac{\overline{W}_\theta}{W_{\mathrm{inj}}} \tag{1}$$

assuming no mass air flow (MAF) sensor drifts or errors in fuel injection. The SAFR ethanol estimation is also based on the following two basic relations. First, let e denote the volume fraction of ethanol in gasoline-ethanol blend. And let e_m denote the mass fraction of ethanol. Then, e_m is expressed as:

$$e_m = \frac{e\rho_{\mathrm{eth}}}{e\rho_{\mathrm{eth}} + (1-e)\rho_{\mathrm{gsl}}} = \frac{e}{e + \frac{(1-e)\rho_{\mathrm{gsl}}}{\rho_{\mathrm{eth}}}} = \frac{e}{e + \frac{(1-e)}{1.056}} \tag{2}$$

where $\rho_{\mathrm{eth}} = 789$ kg/m^3 and $\rho_{\mathrm{gsl}} = 747$ kg/m^3 denote the density of ethanol and the density of gasoline, respectively. Second, the stoichiometric air-to-fuel ratio for flex fuel is expressed as

$$\mathrm{AFR}_s = 9 \times e_m + 14.6 \times (1 - e_m). \tag{3}$$

Hence, the volume fraction of ethanol, e, is calculated from an estimated stoichiometric AFR, $\widehat{\mathrm{AFR}}_s$, through the e_m

$$\widehat{e}_m = \frac{14.6 - \widehat{\mathrm{AFR}}_s}{5.6} \tag{4}$$

$$\widehat{e} = \frac{\widehat{e}_m}{1.056 - 0.056 \times \widehat{e}_m}. \tag{5}$$

B. Dynamic SAFR-Based Ethanol Estimation

Although the AFR regulation to its stoichiometric value is very fast, it is clear from (4)-(5) that the ethanol estimation needs to tune-out λ excursions due to load changes. The basic SAFR principle described above can be augmented with an add-on filter or the basic SAFR scheme can be slightly modified using adaptive control principles instead of being a static function of the measured fuel and air measurement to account for these load-induced λ excursions. To design this dynamic SAFR-based ethanol estimation scheme the full system dynamics of the air, the fuel, and the λ regulation need to be considered. Fig. 1 shows the block diagram of AFR control with the proposed dynamic SAFR-based ethanol estimation. Due to the long delays in the λ feedback loop, most engine controllers employ a feedforward fuel command which is primarily derived from the estimated cylinder air charge divided by the assumed stoichiometric ratio of the assumed fuel blend. Furthermore, the feedforward is usually designed to eliminate the transient effects of fuel puddle dynamics [14], [15] in port fuel injected (PFI) engines as shown in Fig. 2. Since the puddle dynamics is dependent on the ethanol content, estimation of ethanol content may also be used for the transient fuel compensation (TFC). A model of fuel puddle dynamics with alternative fuels is discussed in [16]–[18] where a fuel blend is modeled as a certain combination of organic compounds that mimics the distillation behavior of an actual fuel. When the assumed stoichiometric ratio is correct, and there are no errors in the air charge and fuel puddle dynamics estimation, and no drifts or faults in the injector, the feedforward fuel command is then perfect and the feedback fuel compensation should be zero. An estimation algorithm can utilize a nonzero feedback fuel command to adapt and improve the feedforward fuel compensator so that the feedback converges back to its nominal zero value.

In the case of an FFV, the engine management system will have to make a decision and assume that the error arises from changes in the fuel blend or from component (sensor, actuator) aging. The ethanol content estimation is then realized through a fuel adaptation loop by integrating the fuel feedback control signal, W_{fb}

$$\dot{\widehat{\mathrm{AFR}}}_s = -\gamma_e W_{fb} \alpha_{tr} \tag{6}$$

where $\widehat{\mathrm{AFR}}_s$ denotes the estimated stoichiometric AFR of the injected fuel, γ_e is the adaptation gain, α_{tr} is a triggering variable which enables the ethanol estimation by setting it to $\alpha_{tr} = 1$ after detecting a tank refill event. The fuel feedback controller can be emulated by any integral-based controller, and without loss of generality, we assume a simple proportional-integral (PI) feedback control signal

$$W_{fb} = C_{fb}(s)(\lambda^{\mathrm{des}} - \bar{\lambda}) = -k_{\mathrm{PI}} \frac{\tau_{\mathrm{PI}} s + 1}{s}(1 - \bar{\lambda}). \tag{7}$$

To tune the gains γ_e in (6) one has to consider the full dynamic system and the k_{PI} and τ_{PI} of the λ regulation loop as discussed in the next section.

C. Closed-Loop SAFR Estimation System Dynamics

Let us consider the linearized dynamics of the system with the simple AFR estimation law about a fixed stoichiometry and a fixed cylinder air flow associated with a specific load (manifold pressure) and engine speed. Fig. 2 shows the phenomenological process considered once the fuel command W_{inj} is issued to the injectors all the way until λ is measured by the EGO sensor (cylinder block of Fig. 1 including fuel puddle dynamics for a PFI engine). We assume that the fuel puddle dynamic behavior is expressed as a linear time invariant (LTI) transfer function in the neighborhood of the chosen equilibrium point given by

$$G_{fd}(s) = \frac{(1-X)\tau s + 1}{\tau s + 1} \tag{8}$$

[2]Ethanol needs a higher gaseous concentration in air to be flammable, because it does not contain some of gasoline's highly volatile components such as pentane and hexane [12], [13]. Due to these factors, the required fuel flow rate per cycle event during cold start would vary for different gasoline-ethanol blends.

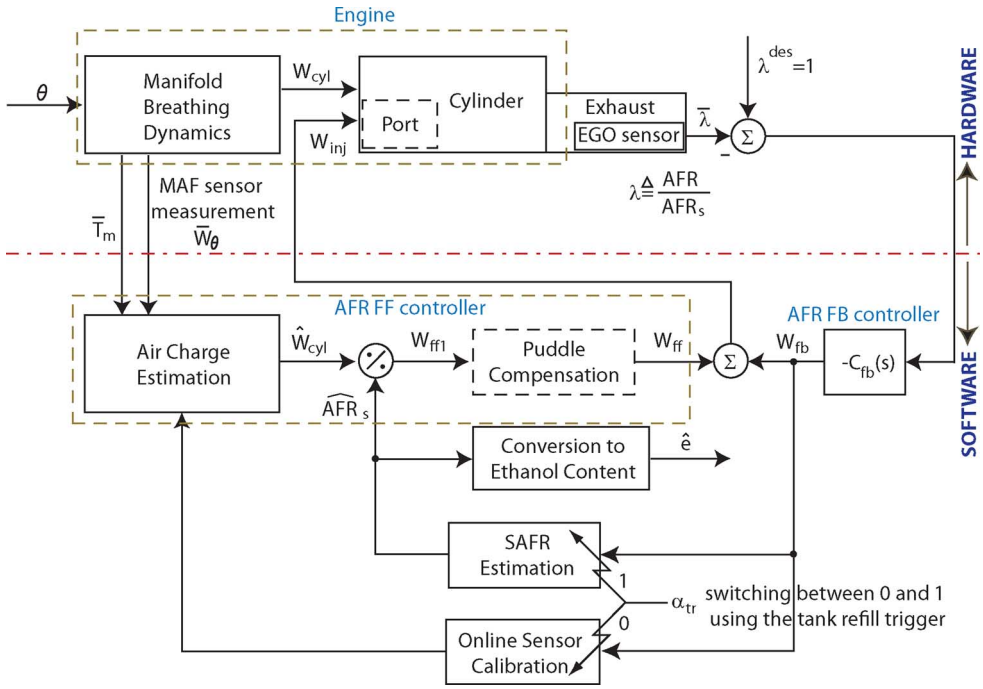

Fig. 1. Block diagram of AFR control.

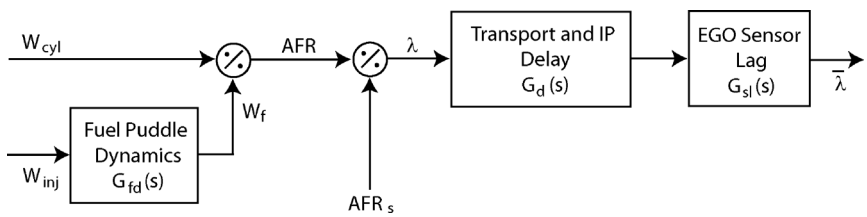

Fig. 2. Path from injector command to EGO sensor output.

where X and τ denote the wall-impacting fraction of the injected fuel and the vaporization time constant of the fuel puddle, respectively [19]. The cylinder input λ is by definition

$$\lambda \triangleq \frac{\left(\frac{W_{\rm cyl}}{W_f}\right)}{\rm AFR_s} \tag{9}$$

where $W_{\rm cyl}$ denotes the air flow rate into the cylinder, W_f the fuel flow rate into the cylinder and $\rm AFR_s$ the stoichiometric air-to-fuel ratio. The quantity W_f is the fuel flow rate that effectively enters the cylinder related with the fuel injection rate, $W_{\rm inj}$, by the fuel dynamics such that

$$W_f = G_{fd}(s) W_{\rm inj}. \tag{10}$$

Let the Padé approximation of the transport and induction-to-power (IP) delay from the cylinder input λ to the exhaust λ be

$$G_d(s) = \frac{1 - \frac{\tau_d}{2}s}{1 + \frac{\tau_d}{2}s} \tag{11}$$

where τ_d is the delay time which depends on engine speed. Let us express the λ sensor lag as

$$G_{sl}(s) = \frac{1}{1 + \tau_s s} \tag{12}$$

where τ_s is the time constant which lumps the chemical, the electrical, and the communication delays of the EGO sensor. The measured λ is then expressed as

$$\bar{\lambda} = G_{sl}(s) G_d(s) \lambda. \tag{13}$$

Let us define $G(s)$ as

$$G(s) \triangleq G_{fd}(s) G_d(s) G_{sl}(s). \tag{14}$$

The control law without the feedforward compensation of the fuel dynamics can be summarized as

$$W_{\rm inj} = W_{ff} + W_{fb} \tag{15}$$

$$W_{ff} = \frac{\widehat{W}_{\rm cyl}}{\widehat{\rm AFR}_s} \tag{16}$$

$$W_{fb} = C_{fb}(s)(1 - \bar{\lambda}) \tag{17}$$

$$\dot{\widehat{\rm AFR}}_s = -\gamma_e W_{fb} \tag{18}$$

where the feedback controller, $C_{fb}(s)$, is assumed to be a PI controller as in (7). Note that here the air flow rate into the cylinder is assumed to be exactly estimated, $\widehat{W}_{\rm cyl} \equiv W_{\rm cyl}$, for the PI gain tuning analysis in C_{fb} (7). The closed-loop system is expressed by the set of equations of (9), (10), (13), and (15)–(18).

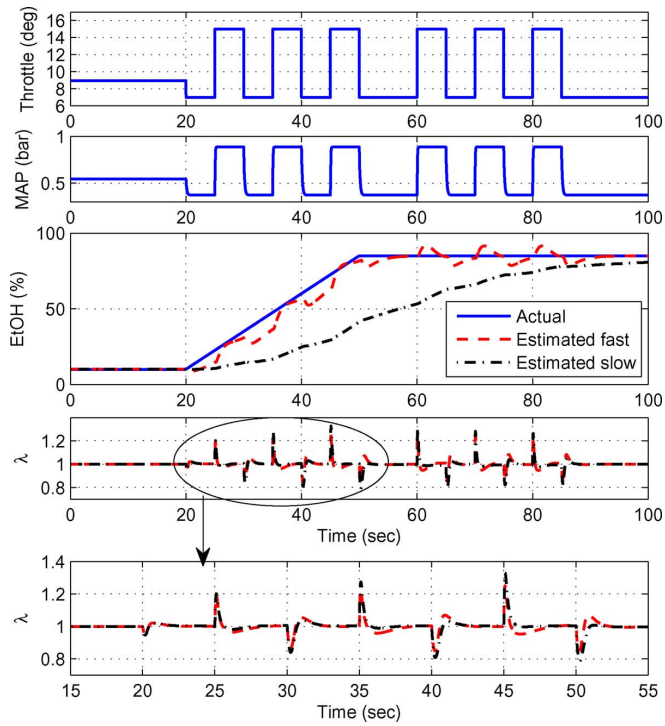

Fig. 3. Simulated example of fast and slow ethanol estimations.

The ability of the overall system to regulate λ and to estimate the actual AFR_s is shown in detail in the Appendix along with a tuning approach for the three gain γ_e and the k_{PI} and τ_{PI} given the engine dynamics.

Fig. 3 illustrates a simulated example of ethanol estimation with different estimator gains under the same operating scenarios. The engine model introduced by Crossley and Cook [20] was utilized while maintaining the engine speed at 2000 RPM for throttle-to-cylinder air charge dynamics assuming that the rotational dynamics are much slower than the mass air flow and pressure dynamics. In the simulation, the fast estimation used the estimator gain $\gamma_e = 5000$ selected in Appendix while the slow estimation used $\gamma_e = 500$. The actual ethanol content changed from 10% to 85% and several throttle step changes were applied during the ethanol content change. No MAF sensor error was introduced in the simulation. This example illustrates the following problem associated with slow ethanol estimation. If the car has stopped (engine turned off) at the 60th second or after 1/2 min of running after refueling, the slow ethanol estimation would have had stopped with an E50 instead of E85 value. An example of such a stop immediately after refueling is fueling stations at a rest stop. Cold start with assumed E50 instead of the accurate E85 could have been a problem.

As a solution, one would think that fast ethanol estimation is necessary to avoid the above problems by shortening the period of ethanol content estimation. However, speeding up the ethanol estimation introduces another problem from the strong interaction between throttle-induced λ excursions and ethanol estimation. This interaction is clearly shown in the ethanol estimation plot in Fig. 3 associated with fast ethanol estimation: the ethanol estimation shows significant transient responses caused by throttle changes (or λ excursions). The overall difficulties of tuning the simple simultaneous ethanol estimator and AFR regulator are discussed in the Appendix. We concentrate next in an even harder and more important problem, namely, the ethanol estimation during a MAF sensor drift.

III. Sensitivity of SAFR-Based Ethanol Estimation

This section assumes that the adaptive law (18) and the PI loop (17) converge at steady state and $\lambda_{ss} = 1$ (lambda regulation is achieved). Suppose that a faulty MAF sensor is used and assume there is neither injector fault nor EGO sensor error. Let f_e be the MAF sensor error fraction such that $\overline{W}_\theta = (1 + f_e)W_\theta$, where $\overline{W}_\theta$ is the measured mass air flow through the throttle and W_θ is the actual. The estimated air flow rate into the cylinder in the steady state is then also expressed as

$$\widehat{W}_{\mathrm{cyl}} = (1 + f_e)W_{\mathrm{cyl}}. \tag{19}$$

The fuel injection or fuel flow rate into the cylinder is solely determined by the feedforward command in the steady state

$$W_f = \frac{\widehat{W}_{\mathrm{cyl}}}{\widehat{\mathrm{AFR}}_s}. \tag{20}$$

Due to the λ PI-based feedback loop, λ is regulated at unity, and consequently, the actual steady-state AFR is regulated at the stoichiometric value independently of the fuel

$$\mathrm{AFR}_s = \mathrm{AFR} = \frac{W_{\mathrm{cyl}}}{W_f} = \frac{W_{\mathrm{cyl}}}{\widehat{W}_{\mathrm{cyl}}} \cdot \widehat{\mathrm{AFR}}_s = \frac{1}{1 + f_e}\widehat{\mathrm{AFR}}_s. \tag{21}$$

If the stoichiometric air-to-fuel ratio is expressed by the mass fraction of ethanol, the following equation is obtained:

$$\frac{9 \times e_m + 14.6 \times (1 - e_m)}{9 \times \hat{e}_m + 14.6 \times (1 - \hat{e}_m)} = \frac{1}{1 + f_e} \tag{22}$$

where e_m and $\hat{e}_m$ are the actual mass fraction of ethanol and the estimated mass fraction of ethanol, respectively. The estimated mass fraction of ethanol, $\hat{e}_m$, is then expressed as a function of f_e and e_m

$$\hat{e}_m = e_m - f_e\left(\frac{14.6}{5.6} - e_m\right). \tag{23}$$

The estimated volume fraction of ethanol, $\hat{e}$ can be then calculated by (5).

Fig. 4 shows the volumetric ethanol content estimation with 5% MAF sensor error. The MAF sensor error fraction is amplified to ethanol content error by factor of about 2.6 for E0 and of about 1.8 for E85, respectively.

Simulations were performed to see the transient closed loop system response with simultaneous sensor errors. Errors in air-charge estimation, mass air flow (MAF) sensor and manifold temperature sensor were introduced with an error factor of 5% separately and at a time to check the sensitivity of the ethanol estimation.

The PI control gains and the estimator gain were determined as discussed in Appendix: $\tau_{\mathrm{PI}} = 0.3$, $k_{\mathrm{PI}} = 0.0015$, and $\gamma_e = 5000$. The poles corresponding to the selected gains are marked as points on the root loci of Figs. 17 and 18 in Appendix.

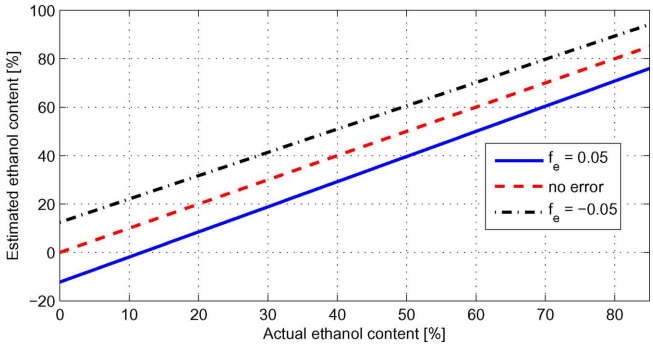

Fig. 4. Ethanol content estimation in the steady state with 5% MAF sensor error.

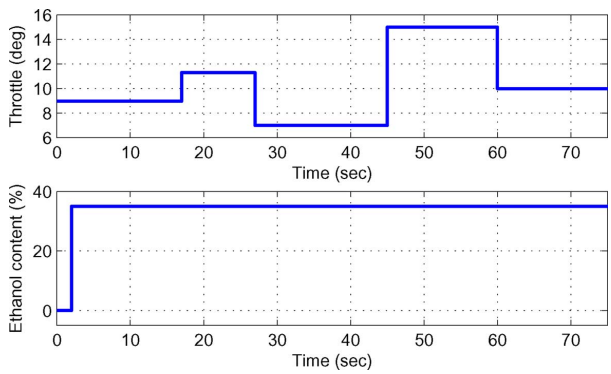

Fig. 5. Simulation input.

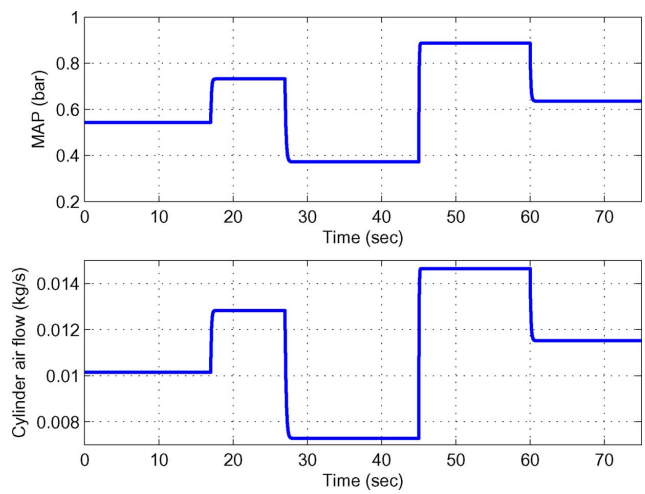

Fig. 6. Manifold absolute pressure and air flow rate into the cylinder induced by throttle input.

Fig. 5 shows the simulation input. Throttle angles were modulated with a sequence of step changes and also a step change of real ethanol content was applied. Initially the fuel used is gasoline and then it is changed to E35. Because of this fuel change, different fuel dynamics parameters were used during the time span of E35 to account for the dynamic dependency on the fuel composition:

- $X_{E35} = 0.361$;
- $\tau_{E35} = 0.4287$.

Fig. 6 shows the change in the manifold absolute pressure and the air flow rate into the cylinder induced by the throttle change.

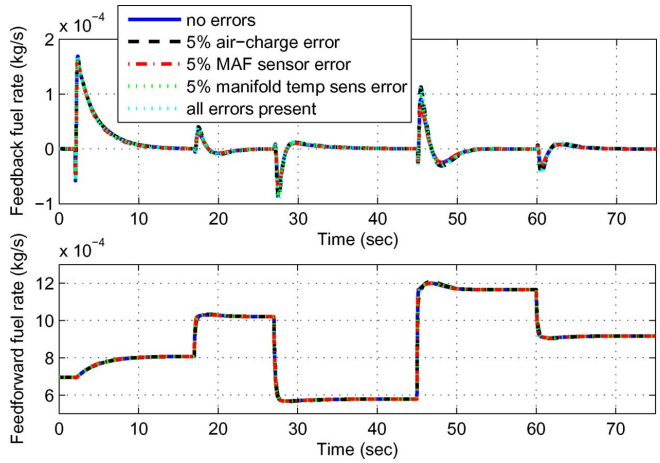

Fig. 7. Simulated feedback fuel signal and feedforward fuel signal.

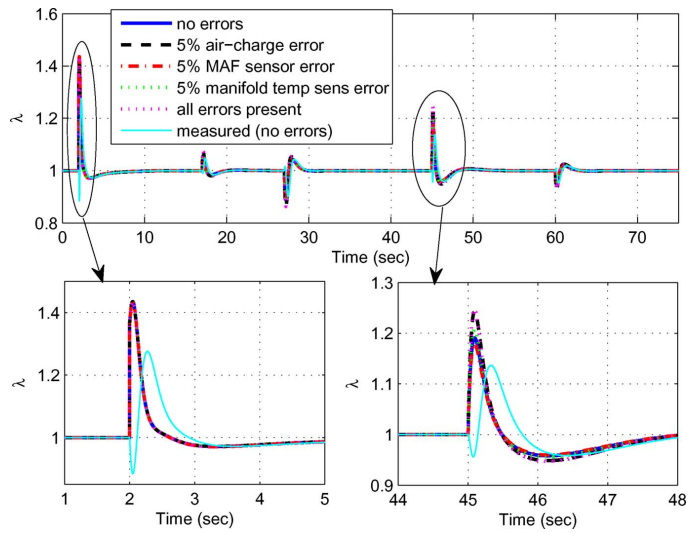

Fig. 8. Simulated λ.

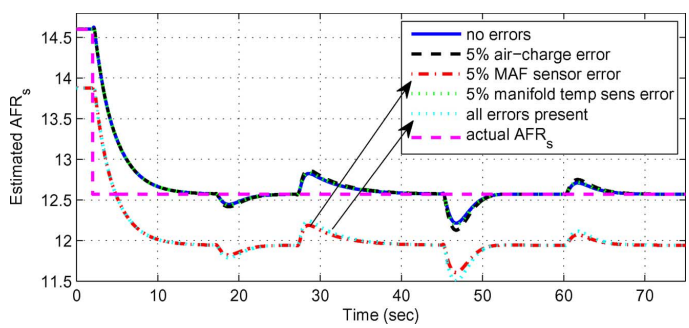

Fig. 9. Simulated stoichiometric AFR estimation.

Figs. 7–10 show the simulation results. The relative air-to-fuel ratio λ and the estimated ethanol content asymptotically track their desired values. The λ error is very sensitive to an air-charge error. It is also moderately sensitive to manifold temperature sensor error, whereas, it is insensitive to MAF sensor error. The estimated stoichiometric AFR or the estimated ethanol content converges to the actual value except for the case of MAF sensor error where the steady-state ethanol percent estimation shows a 30% sensitivity.

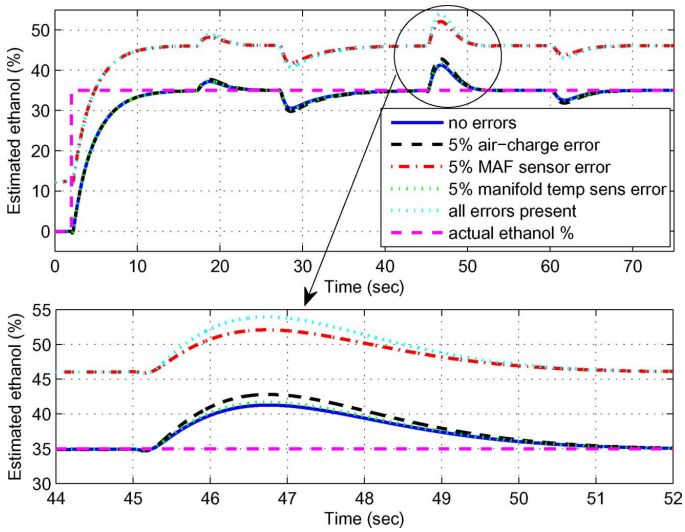

Fig. 10. Simulated ethanol content estimation.

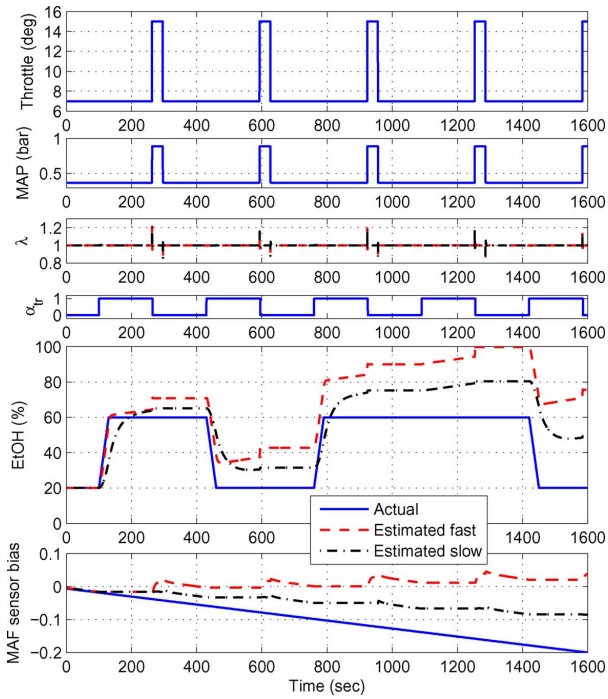

Fig. 11. Simulated example of switching estimations of ethanol and MAF sensor drift with fast and slow ethanol estimations.

A. Switching Adaptation

The triggering variable α_{tr} in Fig. 1 may be used to deactivate the ethanol adaptation ($\alpha_{tr} = 0$) and activate the other adaptation loop that corrects the engine maps and/or drifts in sensors and actuators.

Fig. 11 shows a simulated example of conventional switching estimations of ethanol content and MAF sensor drift. In the simulation, the actual fuel changes between E20 and E60 are exaggerated to show qualitatively what would happen after many refueling. We also assume that the MAF sensor error fraction f_e drifts from 0 to -0.2. The switching variable α_{tr} changed properly between 0 and 1, where $\alpha_{tr} = 1$ selected the ethanol content estimation and $\alpha_{tr} = 0$ the MAF sensor error fraction (or bias) estimation, respectively. In Fig. 11, $\alpha_{tr} = 1$ around 1200 s simulates ethanol detection by refueling event without actual change of ethanol contents. Again, fast and slow ethanol estimations were simulated with the same operating scenarios. Let us first look at the estimation results in Fig. 11 associated with slow ethanol estimation. The MAF sensor drift occurring during the ethanol estimation periods is unobservable and it is incorrectly allocated in the ethanol estimation, hence the accuracy of the ethanol estimation is reduced proportionally to the duration of the estimation period.

In the second example in Fig. 11, the estimation results associated with fast ethanol estimation is even poorer because the transient responses induced by the throttle changes were not accounted for at the transition moments from ethanol content estimation to MAF sensor drift estimation.

The solution to this problem would be a more comprehensive criterion for switching ethanol estimation on and off. The new switching criterion would involve monitoring throttle variability and switching between the two estimations only when steady-state driving has been achieved. This solution is practically equivalent with having a slow ethanol estimation with a longer ethanol estimation period where the MAF sensor drifts are unobservable and misallocated in estimated ethanol.

We propose a cylinder air flow estimation scheme independent of the ethanol estimation in the following sequel, where the MAF sensor drift is estimated using additional manifold absolute pressure measurements.

IV. Speed-Density Method

In order to avoid problems in the switching adaptation discussed in Section III-A, the cylinder air flow should be estimated and account for the MAF sensor drift, independently of λ measurement. For this purpose, an intake manifold pressure sensor may be utilized. Using a manifold absolute pressure (MAP) sensor may be suitable in the sense that the associated cost is low. A conventional method from which the cylinder air flow can be calculated using MAP is the *speed-density* method

$$W_{\rm cyl} = \eta_v \frac{n_e}{2} V_d \frac{p_m}{RT_m} \tag{24}$$

where p_m denotes the manifold absolute pressure, η_v is the volumetric efficiency, n_e is the engine speed (in rps), and V_d is the total displaced cylinder volume. Since η_v bears relatively high uncertainty, estimating cylinder air flow only using the MAP measurement via this equation is not a good idea. Therefore, we will still use the MAF sensor measurement and the drift will be compensated by the MAP measurement via the speed density equation. Note that any error fraction in MAP results in the same amount of error fraction in cylinder air flow from the nominal speed-density equation

$$\frac{\delta W_{\rm cyl}}{W_{\rm cyl}} = \frac{\delta p_m}{p_m} \tag{25}$$

where nominal speed-density equation assumes that the volumetric efficiency, η_v is independent of MAP, p_m, i.e., not a function of p_m, which is not strictly true in some real engines though. Therefore, the potential ethanol estimation error during MAP drift may not be worse than the ethanol estimation error during

MAF drift. Moreover, MAP sensor accuracy is usually much better than MAF sensor accuracy [21], [22]. This fact justifies the idea of using MAP sensor to correct MAF sensor drift.

V. High Gain Observer for Input Estimation

The purpose of this section is to review the input estimation algorithm that will be used in subsequent sections for correcting MAF sensor drifts. Stotsky and Kolmanovsky have applied the following high gain observer technique to cylinder air charge estimation using a manifold pressure sensor [23]. Their work serves as a basis for the compensation of MAF sensor drift in this paper.

We consider an input estimation problem arising from a first-order dynamic system

$$\dot{z} = y + x \tag{26}$$

where the signals z and y are measured, but x is a unknown time-varying input which has to be estimated on line. A high gain observer is defined in terms of auxiliary variables ϵ and v such that the estimation of x is given by

$$\hat{x} = \gamma z - v \tag{27}$$

where

$$\epsilon \triangleq \hat{x} - x = \gamma z - v - x \tag{28}$$

and v satisfies

$$\dot{v} = -\gamma v + \gamma y + \gamma^2 z. \tag{29}$$

Here γ is a positive observer gain. Evaluating the derivative of v along the solutions of system (28) one obtains

$$\dot{\epsilon} = -\gamma\epsilon - \dot{x}. \tag{30}$$

Assume now that $\dot{x}$ is bounded, i.e., that there exists a positive constant b_1 such that $\sup_t \|\dot{x}(t)\| \leq b_1$. Multiplying (30) by 2ϵ, and using an estimate $\|2\dot{x}\epsilon\| \leq \dot{x}^2/\gamma + \gamma\epsilon^2$ it follows that $d\epsilon^2/dt \leq -\gamma\epsilon^2 + b_1^2/\gamma$ and the following transient bound for the estimation error is obtained:

$$\|\epsilon(t)\| \leq \sqrt{\epsilon(0)^2 e^{-\gamma t} + \frac{b_1^2}{\gamma^2}}. \tag{31}$$

Transient bound (31) implies that the upper bound on the estimation error for any $t > 0$ can be made arbitrarily small by increasing the design parameter $\gamma > 0$. Note that if one defines $\hat{z} = v/\gamma$, then (29) reduces to $\dot{\hat{z}} = -\gamma(\hat{z} - z) + y$. Thus $\hat{z}$ can be viewed as an estimate of z, provided $\gamma > 0$ is sufficiently large.

The same result can be obtained by filtering both sides of (26) with a low pass filter [23].

VI. Estimation of Flow Through the Throttle

A. MAF Sensor Dynamics Including Drift

The MAF sensor dynamics can be described by a first-order lag [24]

$$\dot{\overline{W}}_\theta = -\frac{1}{\tau_{MAF}}(\overline{W}_\theta - W_\theta) \tag{32}$$

where τ_{MAF} is the MAF sensor time constant, W_θ is the actual flow through the throttle, and $\overline{W}_\theta$ is the measured flow through the throttle by the MAF sensor.

The MAF sensor dynamics with drift can be modeled through a biased sensor gain

$$\dot{W}_{\theta,n} = -\frac{1}{\tau_{\mathrm{MAF}}}(W_{\theta,n} - W_\theta) \tag{33}$$

$$\overline{W}_\theta = (1 + C)W_{\theta,n} \tag{34}$$

where $W_{\theta,n}$ is the mass air flow through the throttle body of the nominal system and C is a parameter that affects the MAF sensor gain.

The MAF sensor dynamics is then expressed as

$$\dot{\overline{W}}_\theta = -\frac{1}{\tau_{\mathrm{MAF}}}\left(\overline{W}_\theta - (1 + C)W_\theta\right). \tag{35}$$

B. Throttle Flow Estimation

To estimate the input, W_θ, the high gain observer previously discussed is utilized. Equation (35) is exactly (26) with $z = \overline{W}_\theta$, $y = -(1/\tau_{\mathrm{MAF}})\overline{W}_\theta$ and $x = (1/\tau_{\mathrm{MAF}})(1 + C)W_\theta$. Thus, we apply the input observer, (29) and (27), to (35)

$$\dot{v}_f = -\gamma_f v_f - \frac{\gamma_f}{\tau_{\mathrm{MAF}}}\overline{W}_\theta + \gamma_f^2 \overline{W}_\theta \tag{36}$$

$$\widehat{W}_C = \tau_{\mathrm{MAF}}(\gamma_f \overline{W}_\theta - v_f) \tag{37}$$

where W_C is defined as

$$W_C \triangleq (1 + C)W_\theta \tag{38}$$

$\widehat{W}_C$ is the estimation of W_C and γ_f is an observer gain. If we know the sensor drift C, from the adaptation in Section VIII, we can estimate W_θ

$$\widehat{W}_\theta = \frac{\widehat{W}_C}{(1 + C)} \tag{39}$$

where $\widehat{W}_\theta$ is the estimation of W_θ.

VII. Estimation of Engine Cylinder Flow

This section restates the same observer design as discussed in [23], which utilizes an intake MAP sensor to estimate the engine cylinder flow. The same observer can be effectively utilized to compensate for the volumetric efficiency variation caused by ethanol content variation in gasoline-ethanol blended fuel, regardless whether the variation is indeed large or not.

A. Manifold Filling Dynamics

The intake manifold filling dynamics is modeled as an isothermal intake manifold pressure model

$$\dot{p}_m = \frac{RT_m}{V_m}(W_\theta - W_{\mathrm{cyl}}). \tag{40}$$

A conventional technique for estimating the cylinder flow into a spark ignition (SI) engine involves a *speed-density* (24). The volumetric efficiency bears uncertainty and it may be calibrated by the engine dynamometer test. In any case, the cylinder air

flow can be viewed as a sum of nominal cylinder flow and an uncertainty term

$$W_{\rm cyl} = W_{{\rm cyl},n} + \Delta W_{\rm cyl} \tag{41}$$

with the nominal cylinder flow $W_{{\rm cyl},n}$ expressed as a function of MAP, p_m, engine speed, n_e, and possibly ethanol content in the fuel blend, e

$$W_{{\rm cyl},n} = \mathcal{W}_{{\rm cyl},n}(p_m, n_e, e). \tag{42}$$

The intake manifold filling dynamics, (40), then becomes

$$\dot{p}_m = \frac{RT_m}{V_m}(W_\theta - W_{{\rm cyl},n}) - \frac{RT_m}{V_m}\Delta W_{\rm cyl}. \tag{43}$$

B. Cylinder Flow Estimation

Equation (43) is exactly the same as (26) with $z = p_m$, $y = (RT_m/V_m)(W_\theta - W_{{\rm cyl},n})$, $x = -(RT_m/V_m)\Delta W_{\rm cyl}$. By applying the high gain observer, (29) and (27), to (43), the following input observer is obtained:

$$\dot{v} = -\gamma v + \gamma\frac{RT_m}{V_m}(W_\theta - W_{{\rm cyl},n}) + \gamma^2 p_m \tag{44}$$

$$\widehat{\Delta W}_{\rm cyl} = \frac{V_m}{RT_m}(v - \gamma p_m) \tag{45}$$

where $\widehat{\Delta W}_{\rm cyl}$ is the estimation of $\Delta W_{\rm cyl}$ and γ is an observer gain. The cylinder flow estimation is then expressed as

$$\widehat{W}_{\rm cyl} = W_{{\rm cyl},n} + (v - \gamma p_m)\frac{V_m}{RT_m} \tag{46}$$

$$\dot{v} = -\gamma\frac{RT_m}{V_m}(\widehat{W}_{\rm cyl} - W_\theta). \tag{47}$$

The intake manifold absolute pressure sensor is fast but may give noisy signals. A low pass filter can be utilized to filter out such noise. The isothermal intake manifold pressure model, (40), is used to avoid an excessive phase lag. Based on (40), a low pass filter can then be developed if W_θ and $W_{\rm cyl}$ are known

$$\dot{\hat{p}}_m = \frac{RT_m}{V_m}(W_\theta - W_{\rm cyl}) + \gamma_p(\bar{p}_m - \hat{p}_m) \tag{48}$$

where $\hat{p}_m$ is the estimated intake manifold absolute pressure and $\bar{p}_m$ is the measured pressure by the intake manifold absolute pressure sensor. Observers (47), (46), and (48) are combined to yield one observer scheme. In (47) and (46), the manifold absolute pressure, p_m, is replaced by the filtered manifold absolute pressure, $\hat{p}_m$. In (48), the cylinder flow, $W_{\rm cyl}$, is replaced by the estimated cylinder flow, $\widehat{W}_{\rm cyl}$. The combined observer is then summarized as

$$\dot{v} = -\gamma\frac{RT_m}{V_m}(\widehat{W}_{\rm cyl} - W_\theta) \tag{49}$$

$$\widehat{W}_{\rm cyl} = \mathcal{W}_{{\rm cyl},n}(\hat{p}_m, n_e, e) + (v - \gamma\hat{p}_m)\frac{V_m}{RT_m} \tag{50}$$

$$\dot{\hat{p}}_m = \frac{RT_m}{V_m}(W_\theta - \widehat{W}_{\rm cyl}) + \gamma_p(\bar{p}_m - \hat{p}_m). \tag{51}$$

VIII. MAF Sensor Drift Adaptation

The drift parameter C needs to be known to obtain the estimation of the throttle flow, $\widehat{W}_\theta$, in (39). If we can estimate the cylinder flow, $W_{\rm cyl}$, independently of the MAF measurement, the throttle flow, W_θ, can be estimated using (40) with MAP measurement. Equation (40) is exactly the same as (26) with $z = p_m$, $y = -(RT_m/V_m)W_{\rm cyl}$ and $x = (RT_m/V_m)W_\theta$. Thus, we may apply the input observer, (29) and (27), to (40). The nominal cylinder flow equation, (42), may approximate the original speed-density (24) very well in a limited region of operating conditions. We then use the nominal cylinder flow in applying the input observer

$$\dot{v}_n = -\gamma_n v_n - \gamma_n\frac{RT_m}{V_m}W_{{\rm cyl},n} + \gamma_n^2 p_m \tag{52}$$

$$\widehat{W}_{\theta,\mathcal{W}} = \frac{V_m}{RT_m}(\gamma_n p_m - v_n). \tag{53}$$

Introducing a triggering variable, β_{tr}, the following drift parameter adaptation can be utilized:

$$\dot{\widehat{C}} = \gamma_C(\widehat{W}_C - (1 + \widehat{C})\widehat{W}_{\theta,\mathcal{W}})\beta_{tr} \tag{54}$$

where β_{tr} is 1 in a limited region of operating conditions where the nominal cylinder flow equation is very good to approximate the original speed-density equation and is 0 elsewhere.

IX. Combined Air Charge Adaptation Scheme

The observers discussed so far are combined to yield one observer scheme for cylinder air flow estimation. The throttle flow observer, (36), (37), and (39), the cylinder flow and manifold absolute pressure observer, (49)–(51) and the MAF sensor drift parameter observer, (52), (53), and (54), are combined replacing actual variables by estimated variables

$$\dot{v}_f = -\gamma_f v_f - \frac{\gamma_f}{\tau_{\rm MAF}}\overline{W}_\theta + \gamma_f^2\overline{W}_\theta \tag{55}$$

$$\widehat{W}_C = \tau_{\rm MAF}(\gamma_f\overline{W}_\theta - v_f) \tag{56}$$

$$\widehat{W}_\theta = \frac{\widehat{W}_C}{(1 + \widehat{C})} \tag{57}$$

$$\dot{v} = -\gamma\frac{RT_m}{V_m}(\widehat{W}_{\rm cyl} - \widehat{W}_\theta) \tag{58}$$

$$\widehat{W}_{\rm cyl} = \widehat{W}_{{\rm cyl},n} + (v - \gamma\hat{p}_m)\frac{V_m}{RT_m} \tag{59}$$

$$\dot{\hat{p}}_m = \frac{RT_m}{V_m}(\widehat{W}_\theta - \widehat{W}_{\rm cyl}) + \gamma_p(\bar{p}_m - \hat{p}_m) \tag{60}$$

$$\widehat{W}_{{\rm cyl},n} = \mathcal{W}_{{\rm cyl},n}(\hat{p}_m, n_e, e) \tag{61}$$

$$\dot{v}_n = -\gamma_n v_n - \gamma_n\frac{RT_m}{V_m}\widehat{W}_{{\rm cyl},n} + \gamma_n^2\hat{p}_m, \tag{62}$$

$$\widehat{W}_{\theta,\mathcal{W}} = \frac{V_m}{RT_m}(\gamma_n\hat{p}_m - v_n) \tag{63}$$

$$\dot{\widehat{C}} = \gamma_C(\widehat{W}_C - (1 + \widehat{C})\widehat{W}_{\theta,\mathcal{W}})\beta_{tr}. \tag{64}$$

X. Steady-State Analysis

The proposed fifth-order observer uses MAP, MAF, n_e and an estimated ethanol content to derive a feedforward fuel calculated, $W_{ff1} = \widehat{W}_{\rm cyl}/\widehat{\rm AFR}_s$, that accounts for the MAF sensor drift. The estimated ethanol is still based on (6). We omit the stability analysis although this can be achieved using a Lyapunov-like function as in [23] or evaluating closed-loop observer eigenvalues of the linearized system for selection of the five available gains. In this section, we evaluate the proposed scheme and the errors it can introduce. Its potential drawbacks are highlighted in order to critically evaluate its potential contributions. For steady-state analysis, we assume that there is no noise in MAP measurement, i.e., $\bar{p}_m = p_m$. The calculation is straightforward by setting all state equations or all state derivatives to zero. In equilibrium computation, the state (64) is automatically set to zero if $\beta_{tr} = 0$. From all state equations other than (64), the steady-state results are obtained

$$W_\theta = W_{\rm cyl} \tag{65}$$

$$\overline{W}_\theta = \widehat{W}_C = (1+C)W_\theta = (1+C)W_{\rm cyl} \tag{66}$$

$$\hat{p}_m = p_m \tag{67}$$

$$\begin{aligned}\widehat{W}_{\rm cyl} = \widehat{W}_\theta &= \frac{\widehat{W}_C}{(1+\widehat{C})} = \frac{\overline{W}_\theta}{(1+\widehat{C})} \\ &= \frac{1+C}{1+\widehat{C}}W_\theta = \frac{1+C}{1+\widehat{C}}W_{\rm cyl}\end{aligned} \tag{68}$$

$$\widehat{W}_{\theta,\mathcal{W}} = \widehat{W}_{{\rm cyl},n} = W_{{\rm cyl},n}. \tag{69}$$

The steady-state estimation errors are then

$$\widetilde{W}_{\rm cyl} = \widetilde{W}_\theta = \frac{\widehat{C}-C}{1+\widehat{C}}W_{\rm cyl} = -\frac{\widetilde{C}}{1+\widehat{C}}W_{\rm cyl} \tag{70}$$

$$\tilde{p}_m = 0 \tag{71}$$

where estimation errors are defined as $\widetilde{W}_{\rm cyl} \triangleq W_{\rm cyl} - \widehat{W}_{\rm cyl}$, $\widetilde{W}_\theta \triangleq W_\theta - \widehat{W}_\theta$, $\widetilde{C} \triangleq C - \widehat{C}$, and $\tilde{p}_m \triangleq p_m - \hat{p}_m$. From (70), we can consider the following three different special cases.

1) If there is no steady-state error in drift parameter estimation ($\widetilde{C} = 0$), there is no error in cylinder air flow estimation in steady state

$$\widetilde{W}_{\rm cyl}\big|_{\widetilde{C}=0} = 0. \tag{72}$$

This is a desirable result because our estimation purpose is to enhance accuracy of cylinder air flow estimation by correcting MAF sensor drift.

2) Even if there is no MAF sensor drift ($C = 0$), the proposed cylinder estimation will rely on the estimated sensor drift with following cylinder air flow estimation error in steady state:

$$\widetilde{W}_{\rm cyl}\big|_{C=0} = \frac{\widehat{C}}{1+\widehat{C}}W_{\rm cyl}. \tag{73}$$

In this case, if MAF sensor drift compensation fails to estimate the actual value ($C = 0$) correctly, it may cause undesirable cylinder air flow estimation error which would not appear were it not for the drift compensation. Since the drift parameter estimation depends on the accuracy of the nominal cylinder flow expression, (42), and is not always activated according to the switching trigger β_{tr}, misestimation of the drift parameter is not negligible indeed.

3) If there is no MAF sensor drift compensation ($\widehat{C} = 0$), there is the following cylinder air flow estimation error in steady state:

$$\widetilde{W}_{\rm cyl}\big|_{\widehat{C}=0} = -CW_{\rm cyl}. \tag{74}$$

This case corresponds to use of a conventional cylinder flow estimation scheme without any compensation of MAF sensor drift. The estimation error of (74) results in amplified error in ethanol content estimation after all, hence motivating our drift compensation scheme discussed so far.

Equation (73) shows estimation performance degradation unnecessarily caused by using the estimation algorithm proposed in this paper if there is actually no MAF sensor drift at all. However, (74) shows why the proposed algorithm is worth using if the MAF sensor drift is not actually negligible.

In a region of operating conditions where the nominal cylinder flow equation is a very good approximation of actual cylinder air flow, i.e., $\beta_{tr} = 1$, the following equilibrium equation holds from (64):

$$\widehat{W}_C = (1+\widehat{C})\widehat{W}_{\theta,\mathcal{W}}. \tag{75}$$

The following steady-state estimation results are then immediately obtained from (68) and (69):

$$\widehat{W}_{\rm cyl} = \widehat{W}_\theta = W_{{\rm cyl},n}, \quad \widehat{C} = C + (1+C)\frac{\Delta W_{\rm cyl}}{W_{{\rm cyl},n}}. \tag{76}$$

Steady-state estimation errors are then

$$\widetilde{W}_{\rm cyl} = \widetilde{W}_\theta = \Delta W_{\rm cyl}, \quad \widetilde{C} = -(1+C)\frac{\Delta W_{\rm cyl}}{W_{{\rm cyl},n}}. \tag{77}$$

If a cylinder flow equation perfectly fits to the actual cylinder air flow, i.e., $\Delta W_{\rm cyl} = 0$, there will be no errors in cylinder air flow estimation and drift parameter estimation as shown in (77), i.e., $\widetilde{W}_{\rm cyl} = 0$ and $\widetilde{C} = 0$.

XI. Simulations

Simulation of cylinder air flow estimation under MAF sensor drift is performed in the configuration of AFR control with ethanol content estimation as shown in Fig. 1. Note that a measured intake pressure signal is additionally provided to the air charge estimation block in Fig. 1 in this simulation. We use the same manifold breathing dynamics as provided in [20] and the cylinder block is simulated with a fuel puddle model developed for a port fuel injected (PFI) flex-fuel engine [18]. The puddle compensation block is realized by a transient fuel compensator using the fuel puddle model in [18]. In (34), the drift parameter C may actually vary very slowly around zero

$$\overline{W}_\theta = (1+C(t))W_{\theta,n}$$

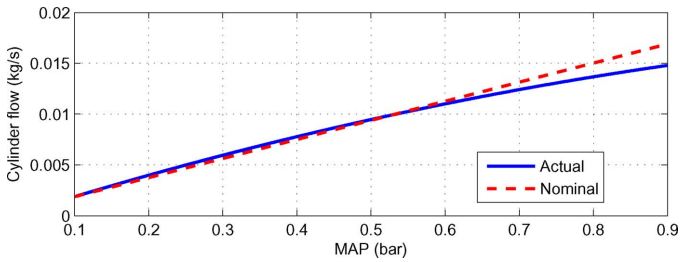

Fig. 12. Cylinder air flow at 2000 RPM.

TABLE II
PARAMETERS AND OBSERVER GAINS USED IN SIMULATION

Parameters	Value	Unit	Gains	Values	Unit
τ_{MAF}	0.02	sec	γ_f	27	sec^{-1}
$\frac{RT_m}{V_m}$	413.28	bar/kg	γ	9	
			γ_p	17	
$\eta_{v,n}\frac{V_d}{V_m}$	0.46554	cycle^{-1}	γ_n	5	
			γ_C	4	

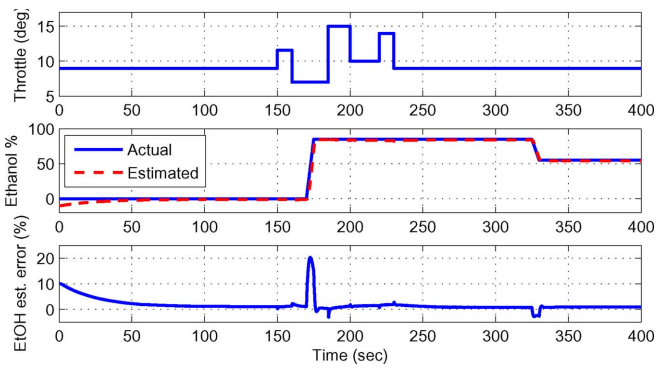

Fig. 13. Simulated inputs and ethanol estimation error.

In this simulation, the following first-order drift model is utilized to give slow variation of drift parameter, $C(t)$:

$$\dot{W}_z = -\frac{1}{\tau_z}(W_z - W_\theta), \quad C = \bar{C}W_z$$

where the drift time constant $\tau_z = 60$ s and the drift gain $\bar{C} = 5.0$ s/kg are used. Fig. 12 shows the cylinder air flow versus manifold absolute pressure, p_m, at a fixed engine rpm used in the simulation. The solid line is for the actual flow, W_{cyl}, and is used in the engine simulation, and the dashed line is the nominal flow, $W_{\text{cyl},n}$, modeled by the nominal speed-density equation and used in the observer. This deviation emulates possible uncertainty in speed-density equation. Note that the nominal cylinder flow is close to the actual around $p_m = 0.5$ bar. Therefore, we assume that the known region of operation conditions for good speed-density approximation is around $p_m = 0.5$ bar for simulation.

Parameters and observer gains used in simulation are summarized in Table II. These gains were tuned by looking at eigenvalues of the linearized closed-loop observer system matrix.

Fig. 13 shows simulated inputs, the throttle angle and the ethanol content. Throttle is modulated with a sequence of several step changes emulating tip-ins and tip-outs. The ethanol content is changed from zero, which means gasoline, to 85% with a ramp profile and then it is changed to 55% later again with a ramp profile. The second plot also depicts the estimated ethanol content which is very sensitive to cylinder air flow estimation error. The third plot shows the ethanol content estimation error. We can observe that the steady-state error is quite allowable actually due to the improved estimation of cylinder air flow. The ethanol content estimation error reduces as time goes by in the first several seconds and this is due to the fact that the estimated drift parameter, $\widehat{C}$, converges closer to the actual as shown in Fig. 15.

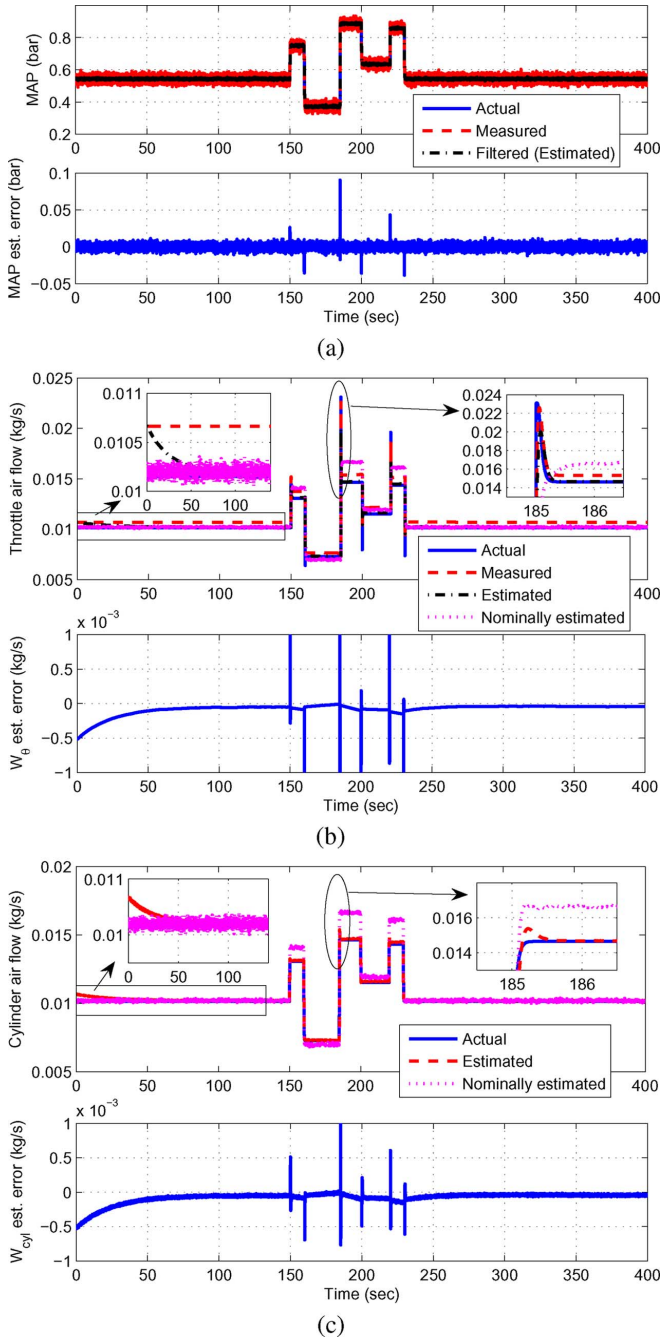

Fig. 14. Estimation result. (a) MAP. (b) Throttle flow. (c) Cylinder air flow.

Fig. 14 shows the estimation results. MAP measurement is corrupted adding white noise to the simulated actual manifold absolute pressure. We can observe reduced noise level in the

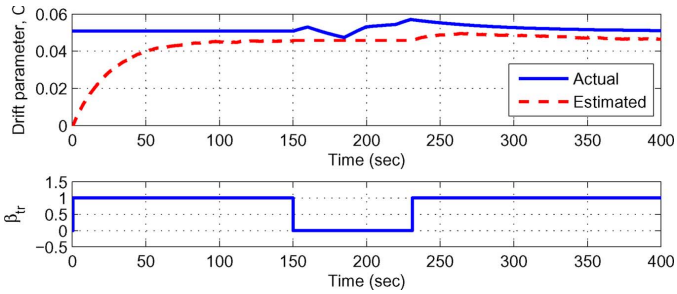

Fig. 15. Drift estimation.

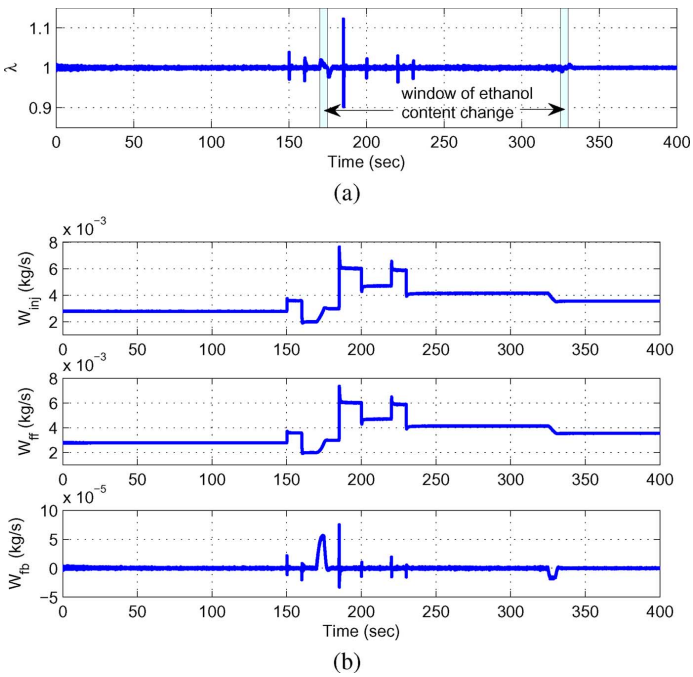

Fig. 16. Simulated λ and fuel injection. (a) Simulated λ. (b) Simulated fuel injection.

filtered pressure signal without much lag in Fig. 14(a). Performance of the throttle air flow estimation and the cylinder flow estimation is quite good. Nominally estimated signals, $\widehat{W}_{\theta,\mathcal{W}}$ and $\widehat{W}_{\mathrm{cyl},n}$, show big errors in operating conditions where the nominal speed-density equation suffers from large deviation from the actual.

Fig. 15 shows the drift parameter estimation and the trigger which changes according to operating conditions. Note that steady-state error in drift parameter estimation remains even if β_{tr} is set to 1 because the (nominal) modeled cylinder flow through the speed density equation differs from the actual cylinder air flow equation. The triggering for this simulation is designed at 2000 engine rpm as

$$\bar{\beta}_{tr}(t) = \begin{cases} 1, & \text{if } 0.4 \text{ bar} \le \hat{p}_m < 0.6 \text{ bar} \\ 0, & \text{otherwise} \end{cases} \tag{78}$$

$$\beta_{tr}(t) = \begin{cases} 1, & \text{if } \bar{\beta}_{tr}(\tau) = 1, \ \ \forall \tau \in [t-0.5, t] \\ 0, & \text{otherwise} \end{cases} \tag{79}$$

to avoid chattering. Fig. 16(a) shows the λ output and Fig. 16(b) shows the controlled fuel injection results. The air-to-fuel ratio is regulated around stoichiometry. The PI feedback signal enables the ethanol content estimation. We can observe that the total fuel injection and feedforward fuel injection increase in the interval of ethanol content change. Again, the ethanol content estimation is always possible as long as the feedback control is activated regardless of MAF sensor drift and uncertainty in speed-density equation. Nevertheless, the accuracy of the ethanol estimation is still degraded if an exact MAF drift compensation is not possible due to significant error in the speed density model with degradation of cylinder air flow estimation.

XII. Conclusion

In this paper, estimation of the ethanol content in flex-fuel vehicles using an AFR-based approach using the stoichiometric AFR control based on λ sensing is demonstrated with a model. The closed-loop dynamics are derived to capture the disturbance rejection characteristic for λ regulation and the associated ethanol estimation error. Tuning of the fuel feedback control and the ethanol estimation gains are shown with root loci and nonlinear simulations.

As the high sensitivity of the AFR-based ethanol content estimation to MAF sensor error is shown, a cylinder air flow estimation scheme that accounts for mass air flow sensor drift or bias is developed in order to avoid misestimation of ethanol content. First, we discuss the consequences, such as possible estimation biases resulting from switching between ethanol and cylinder air flow estimations using an EGO sensor. To obtain a more reliable cylinder air flow estimation by compensating for the MAF sensor drift, the intake manifold pressure sensor signal is utilized together with the speed density principle at selected operating regions. The proposed algorithm involves switching on the correction of MAF sensor drift at operating regions where there is high confidence that the speed density model has high accuracy. Simulation is performed to demonstrate the air flow estimation with the compensation of MAF sensor drift using an intake manifold pressure sensor. In the simulation, the effect of the air flow estimation on the ethanol content estimation in flex fuel vehicles is shown with a realistic assumption of engine modeling accuracy.

Appendix
Tuning of the Basic SAFR Estimation and AFR Controller

A simple tuning approach for the combined AFR regulation and ethanol estimation is provided below. It is shown that although both objectives are simultaneously achieved at steady-state, there is a dynamic coupling that complicates the controller tuning.

The simple dynamic analysis and tuning follows a classical linear control approach. We use the superscript ^{0} to express a nominal value at equilibrium and use δ to express the deviation from the equilibrium. Since we want the estimated stoichiometric AFR, $\widehat{\mathrm{AFR}}_s$, to track the actual stoichiometric AFR, AFR_s, we consider the SAFR estimation error dynamics as well. First, we define the estimation error variable, $\epsilon_{\mathrm{AFR}_s} \triangleq \mathrm{AFR}_s - \widehat{\mathrm{AFR}}_s$.

It is straightforward calculation to obtain the linearized closed-loop dynamics by differentiating system equations with

respect to a nominal set point [25]. The linearized closed-loop dynamics results in

$$\begin{bmatrix} \delta\lambda \\ \delta\epsilon_{\mathrm{AFR}_s} \end{bmatrix} = \begin{bmatrix} T_1(s) & T_2(s) \\ T_3(s) & T_4(s) \end{bmatrix} \begin{bmatrix} \delta W_{\mathrm{cyl}} \\ \delta \mathrm{AFR}_s \end{bmatrix} \tag{80}$$

where the closed-loop transfer functions are

$$T_1(s) = \frac{1}{W^0_{\mathrm{cyl}}} \cdot \frac{X\tau s^3(1+\tau_s s)(1+\frac{\tau_d}{2}s)}{D(s)} \tag{81}$$

$$T_2(s) = -\frac{1}{\mathrm{AFR}^0_s} \cdot \frac{s^2(1+\tau_s s)(\tau s+1)(1+\frac{\tau_d}{2}s)}{D(s)} \tag{82}$$

$$T_3(s) = \frac{1}{W^0_{\mathrm{cyl}}} \cdot \frac{\gamma_e k_{\mathrm{PI}} X\tau s(\tau_{\mathrm{PI}} s+1)(1-\frac{\tau_d}{2}s)}{D(s)} \tag{83}$$

$$T_4(s) = 1 - \frac{1}{\mathrm{AFR}^0_s} \cdot \frac{\gamma_e k_{\mathrm{PI}}(\tau_{\mathrm{PI}} s+1)(\tau s+1)(1-\frac{\tau_d}{2}s)}{D(s)}. \tag{84}$$

with

$$D(s) \triangleq s^2\left(1+\frac{\tau_d}{2}s\right)(1+\tau_s s)(\tau s+1) + k_{\mathrm{PI}} \cdot \left(\frac{\gamma_e}{\mathrm{AFR}^0_s} + \frac{1}{W^0_f}\cdot s\right)((1-X)\tau s+1)\left(1-\frac{\tau_d}{2}s\right)(\tau_{\mathrm{PI}} s+1). \tag{85}$$

It is easy to check that the DC gains of the closed-loop transfer functions, $T_1(s), T_2(s), T_3(s)$, and $T_4(s)$ are all zero with positive gains, which implies the disturbance rejection characteristic for the output AFR regulation ($\delta\lambda$) and for the estimation error $\delta\epsilon_{\mathrm{AFR}_s}$. Therefore, the λ output is asymptotically regulated to unity, ensuring stoichiometric operation, and the estimation of stoichiometric AFR asymptotically converges to the actual stoichiometric AFR if positive gains can be found that guarantee stability and good performance for all the four transfer functions in (80).

PI Gain Tuning of the λ Feedback Controller: For the gain tuning of the feedback PI controller, consider the system of a fixed stoichiometry without the stoichiometric AFR estimation. This is equivalent to setting $\gamma_e = 0$ and $\delta\mathrm{AFR}_s = 0$ in the closed-loop dynamics equation associated with $\delta\lambda$ from (80). The closed-loop dynamic behavior is then expressed as

$$\delta\lambda = \frac{1}{W^0_{\mathrm{cyl}}} \cdot \frac{1-G_{fd}(s)}{1+\frac{1}{W^0_f}G(s)C_{fb}(s)}\delta W_{\mathrm{cyl}}. \tag{86}$$

The variable τ_{PI} in the PI feedback controller can be determined by placing the controller zero to cancel the slowest stable pole of $G(s)$. If the slowest pole is associated with the fuel dynamics, we can set $\tau_{\mathrm{PI}} = \tau$. The root locus with variation of k_{PI} can then be utilized to tune the gain, k_{PI}. Fig. 17 shows the root locus of the closed-loop transfer function with the variation of k_{PI} for a fixed τ_{PI}. To obtain the locus in Fig. 17, the engine parameters were chosen as:

- $X = 0.3$, $\tau = 0.3$ s, $\tau_d = 0.2$ s, $\tau_s = 0.07$ s.

The PI control gains were tuned to

- $\tau_{\mathrm{PI}} = 0.3$, $k_{\mathrm{PI}} = 0.0015$.

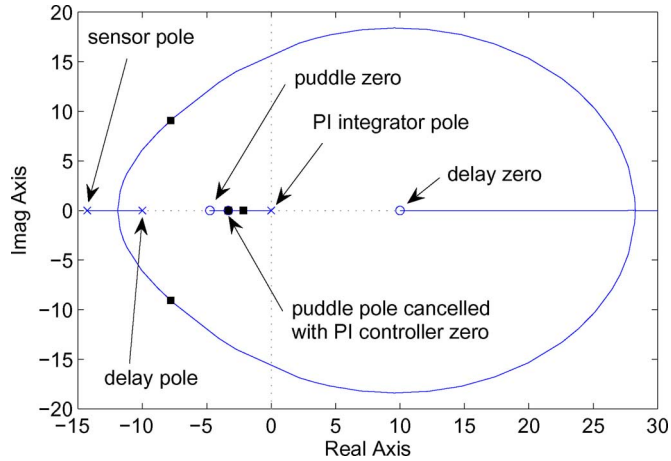

Fig. 17. Root locus with the variation of k_{PI}.

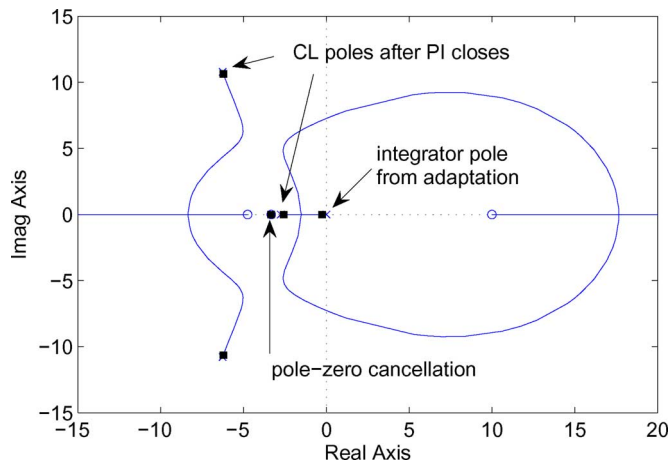

Fig. 18. Root locus with the variation of γ_e.

Ethanol Estimator Gain Tuning: First, the root locus is applied for the $D(s)$ in (85) for a set of fixed feedback gains, τ_{PI} and k_{PI}, determined by the method of the previous subsection. Fig. 18 shows the root locus of the original closed-loop transfer functions with the variation of γ_e for a set of fixed feedback gains previously tuned. The estimator gain γ_e affects the numerator of both transfer functions, $T_3(s)$ and $T_4(s)$, and hence tuning the gain is not clearly explained only with the root locus. However, the estimator gain where the roots cross the imaginary axis in the locus (see Fig. 18) is $\gamma_e = 1.7 \times 10^5$, which determines the range of γ_e for stability. The estimator gain was actually chosen after a few simulations as

- $\gamma_e = 5000$

which is much smaller than the stability bound. Smaller gains may result in slower ethanol adaptations but reducing undesirable transient responses. Implication of different estimator gains has been addressed in Section III-A.

REFERENCES

[1] R. C. Delgado, A. S. Araujo, and V. J. Fernandes Jr., "Properties of Brazilian gasoline mixed with hydrated ethanol for flex-fuel technology," *Fuel Process. Technol.*, vol. 88, no. 4, pp. 365–368, 2007.

[2] K. Nakata, S. Utsumi, A. Ota, K. Kawatake, T. Kawai, and T. Tsunooka, "The effect of ethanol fuel on a spark ignition engine," SAE, Warrendale, PA, Tech. Paper 2006-01-3380, 2006.

[3] J. S. Cowart, W. E. Boruta, J. D. Dalton, R. F. Dona, F. L. Rivard, II, R. S. Furby, J. A. Piontkowski, R. E. Seiter, and R. M. Takai, "Powertrain development of the 1996 Ford flexible fuel Taurus," SAE, Warrendale, PA, Tech. Paper 952751, 1995.
[4] A. Stodart, J. Maher, L. Greger, and J. Carlsson, "Fuel system development to improve cold start performance of a flexible fuel vehicle," SAE, Warrendale, PA, Tech. Paper 982532.
[5] "A literature review based assessment on the impacts of a 20% ethanol gasoline fuel blend on the Australian vehicle fleet," Orbital Engine Co., Balcatta, Western Australia, Report to Environment Australia, 2002.
[6] L. Bromberg, D. R. Cohn, and J. B. Heywood, "Optimized fuel management system for direct injection ethanol enhancement of gasoline engines," U.S. Patent 7 225 787 B2, Jun. 5, 2007.
[7] F. Theunissen, "Percent ethanol estimation on sensorless multi-fuel systems; Advantages and limitations SAE, Warrendale, PA, Tech. Rep. 2003-01-3562, 2003.
[8] K. Ahn, A. G. Stefanopoulou, L. Jiang, and H. Yilmaz, "Ethanol content estimation in flex fuel direct injection engines using in-cylinder pressure measurements," SAE, Warrendale, PA, Tech. Rep. 2010-01-0166, 2010.
[9] K. Ahn, A. G. Stefanopoulou, L. Jiang, and H. Yilmaz, "Ethanol content estimation in flex fuel direct injection engines with fault detection under fuel injector drifts," presented at the IFAC Symp. Adv. Automotive Control (AAC), Munich, Germany, 2010.
[10] Bosch, Gerlingen, Germany, "Automotive Handbook," 5th ed. 2000.
[11] K. Ahn, A. G. Stefanopoulou, and M. Jankovic, "Tolerant ethanol estimation in flex-fuel vehicles during MAF sensor drifts," presented at the ASME 2nd Annu. Dyn. Syst. Control Conf., Hollywood, CA, 2009.
[12] A. J. Markel and B. K. Bailey, *Modelling and Cold Start in Alcohol-Fueled Engines*. Golden, CO: National Renewable Energy Laboratory, 1998.
[13] E. Kane, Y. Huang, D. Mehta, C. Frey, M. Tillerson, Z. Chavis, S. Aithala, R. Matthews, and M. Hall, "Refinement of a dedicated e85 1999 Silverado with emphasis on cold start and cold drivability," SAE, Warrendale, PA, Tech. Rep. 2001-01-0679, 2001.
[14] M. Locatelli, C. H. Onder, and H. P. Geering, "An easily tunable wall-wetting model for PFI engines," SAE, Warrendale, PA, Tech. Rep. 2004-01-1461, 2004.
[15] L. Guzzella and C. H. Onder, *Introduction to Modeling and Control of Internal Combustion Engine Systems*. New York: Springer, 2004.
[16] J. J. Batteh and E. W. Curtis, "Modeling transient fuel effects with alternative fuels," SAE, Warrendale, PA, Tech. Rep. 2005-01-1127, 2005.
[17] K. Ahn, A. G. Stefanopoulou, and M. Jankovic, "Puddle dynamics and air-to-fuel ratio comensation for gasoline-ethanol blends in flex-fuel engines," *IEEE Trans. Control Syst. Technol.*, vol. 18, no. 6, pp. 1241–1253, Nov. 2010.
[18] K. Ahn, A. G. Stefanopoulou, and M. Jankovic, "Fuel puddle model and AFR compensator for gasoline-ethanol blends in flex-fuel engines," presented at the IEEE Veh. Power Propulsion (VPP) Conf., Dearborn, MI, 2009.
[19] C. F. Aquino, "Transient a/f control characteristics of the 5 liter central fuel injection engine," SAE, Warrendale, PA, Tech. Rep. 810494, 1981.
[20] P. R. Crossley and J. A. Cook, "A nonlinear engine model for drivetrain system development," in *Proc. IEE Int. Conf. (Control)*, 1991, pp. 921–925.
[21] Bosch, Gerlingen, Germany, "MAP sensor technical specifications," 2009.
[22] Bosch, Gerlingen, Germany, "HFM2-air mass meter," 2009.
[23] A. Stotsky and I. Kolmanovsky, "Application of input estimation techniques to charge estimation and control in automotive engines," *Control Eng. Pract.*, vol. 10, no. 12, pp. 1371–1383, 2002.
[24] J. Grizzle, J. Cook, and W. Milam, "Improved cylinder air charge estimation for transient air fuel ratio control," in *Proc. Amer. Control Conf.*, 1994, pp. 1568–1573.
[25] K. Ahn, A. G. Stefanopoulou, and M. Jankovic, "Estimation of ethanol content in flex-fuel vehicles using an exhaust gas oxygen sensor: Model, tuning and sensitivity," presented at the ASME 1st Annu. Dyn. Syst. Control Conf., Ann Arbor, MI, 2008.

Kyung-ho Ahn received the B.S. and M.S. degrees in mechanical engineering from POSTECH, Pohang, South Korea, in 1999 and 2001, respectively, and the Ph.D. degree in mechanical engineering from the University of Michigan, Ann Arbor, in 2011.

From 2001 to 2003, he worked as an Engineer on the Unmanned Aerial Vehicle (UAV) Project with Korea Aerospace Industries, Ltd. He was a Senior Researcher with the Institute for Advanced Engineering, South Korea, where he worked on the Grinding Robot Project from 2003 to 2005. Later, he was Technical Staff with the Korea Institute of Science and Technology, where he worked on the Humanoid Robot Project. He joined the Hyundai-Kia Motors R&D Center, Gyeonggi-do, South Korea, in 2011, where he is currently a Senior Researcher in the Powertrain Control Development Team. His current work addresses the control design of gasoline direct injection engines.

Anna G. Stefanopoulou (F'09) received the Diploma in naval architecture and marine engineering from the National Technology University of Athens, Athens, Greece, in 1991, and the Ph.D. degree in electrical engineering and computer science from the University of Michigan, Ann Arbor, in 1996.

She was an Assistant Professor (1998–2000) at the University of California, Santa Barbara, a Technical Specialist (1996–1997) at Ford Motor Company, and a visiting Professor (2006) at ETH, Zurich. Currently, she is a Professor of mechanical engineering with the University of Michigan and the Director of the Automotive Research Center (ARC), a U.S. Army Center of Excellence in Modeling and Simulation of Ground Vehicles. She has 1 book on control of fuel cell power systems, holds 9 U.S. patents, 4 best paper awards, and 150 publications. Her current work addresses the diagnostics, control, and automation issues associated with internal combustion engines and electrochemical processes such as fuel cells and batteries.

Prof. Stefanopoulou is an ASME Fellow (2008).

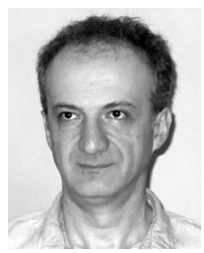

Mrdjan Jankovic (M'94–SM'99–F'04) received the B.S. degree from the University of Belgrade, Yugoslavia, in 1986, and the M.S. and Ph.D. degrees from Washington University, St. Louis, MO, in 1989 and 1992, respectively.

He held postdoctoral teaching and research positions with Washington University and University of California at Santa Barbara. He joined the Ford Research Laboratory, Dearborn, MI, in 1995, where he is currently a Senior Technical Leader in the Powertrain Controls Department. He has coauthored one book, three book chapters, and over 100 technical publications. He is a co-inventor on more than 40 U.S. patents, many of which are implemented in Ford products worldwide.

Dr. Jankovic was a recipient of IEEE Control Systems Technology Award, two Ford Research Technical Achievement Awards, and Best Paper Awards from IEEE, AVEC, and SAE for three automotive control papers. He is a past Associate Editor of the IEEE TRANSACTIONS ON CONTROL SYSTEMS TECHNOLOGY and past chair of several IEEE and SAE committees.